

BISON Validation to In Situ Cladding Burst Test and High-Burnup LOCA Experiments

N. Capps^{1*}, M. Ridley¹, Y. Yan¹, S. Bell^{1,2}, K. Kane^{1,3}

¹Oak Ridge National Laboratory, P.O. Box 2008 1 Bethel Valley Road Oak Ridge, TN 37831

²University of Tennessee, Knoxville, 1331 Circle Park D, Knoxville, TN 37916

³The Johns Hopkins University Applied Physics Laboratory, 11100 Johns Hopkins Rd, Laurel, MD 20723

ABSTRACT

The process for developing and qualifying nuclear fuels for commercial nuclear application requires fundamental material development, characterization, and design; out-of-pile testing on unirradiated materials; integral fuel rod irradiations, testing, and postirradiation examinations; and transient analyses. The historical approach depends on the generation of large empirical datasets and series of integral fuel rod irradiations, and this approach ultimately takes ~20 years—or sometimes longer—to acquire data through extensive sequential testing. Thus, the qualification and eventual deployment of new fuel systems constitute a long process. However, recent technological advancements have provided researchers the opportunity to perform out-of-cell, in situ measurements to assess material performance for the duration of the experiment. One such example of this capability is the use of digital image coordination and thermal imaging to assess Zircaloy cladding performance under a simulated loss-of-coolant accident (LOCA) transient condition. In situ measurements generally provide high-fidelity strain, strain rates, and temperature surface maps. This is critical for the US nuclear industry, which is actively developing a technical basis to support extending the peak rod average burnup from 62 to ~75 GWd/tU and the deployment of accident-tolerant fuel. However, the US Nuclear Regulatory Commission (NRC) outlined in its research information letter several technical issues that the industry must address before extending burnup. One topic of specific interest is understanding the cladding balloon and rupture geometry during the LOCA heat-up phase. By leveraging these advanced in situ capabilities, this work used in situ data generated from a simulated LOCA to better understand high-temperature creep and its effect on Zircaloy balloon and rupture performance. This work used the BISON fuel performance code to assess the high-temperature creep model predictions with in situ data.

1. INTRODUCTION

Loss-of-coolant accidents (LOCAs) are one of the most severe design basis events that a nuclear power plant can experience. They are core-wide events that affect all fuel rods. A LOCA occurs when the primary coolant system suffers a catastrophic failure, resulting in the loss of reactor coolant. LOCAs are divided into three subcategories: small, medium, and large break LOCAs. The most severe and least probable accident-initiating event is a double-ended guillotine break between the reactor vessel and main circulation pump. An example of a pressurized water reactor (PWR) fuel rod response during a double-ended guillotine break is illustrated in Figure 1 [1]. Following the rupture of the cold leg, reactor coolant flashes to steam and blows down through the ruptured opening. Fission product decay heat continues to heat the fuel and reactor internals in the wake of coolant loss, further motivating the need to establish long-term cooling to mitigate the accident. Reactor depressurization occurs from LOCA initiation and completed discharge ~20–30 s into the transient. Once depressurized, the emergency core cooling system (ECCS) initiates to successfully pump water into the reactor primary vessel. Initially, the ECCS is unable to provide sufficient cooling to the fuel elements, and during this time interval, decay heat continues to increase fuel rod temperatures [1] so that permanent fuel damage may occur (i.e., ballooning, burst, and

* Corresponding author: cappsna@ornl.gov

This manuscript has been authored by UT-Battelle, LLC under Contract No. DE-AC05-00OR22725 with the US Department of Energy (DOE). The US government retains and the publisher, by accepting the article for publication, acknowledges that the US government retains a nonexclusive, paid-up, irrevocable, worldwide license to publish or reproduce the published form of this manuscript, or allow others to do so, for US Government purposes. DOE will provide public access to these results of federally sponsored research in accordance with the DOE Public Access Plan (<http://energy.gov/downloads/doe-public-access-plan>).

ultimately oxidation and hydriding), resulting in the loss of post-quench ductility (PQD) [2]. Several conditions related to the local fuel rod and assembly conditions govern the severity of the LOCA transient. For example, the pre-transient rod power governs fuel rod decay heat; radial heat transfer across the pellet, gap, and cladding; external fuel rods acting as additional heat sources; and pre-transient and transient thermal hydraulic conditions. The ECCS response also is critical to governing LOCA performance.

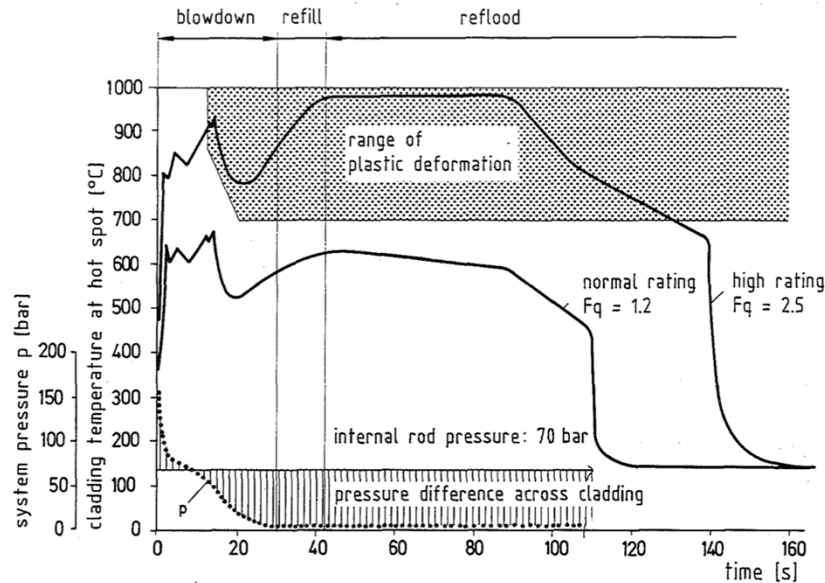


Figure 1. Generic description of Zircaloy-4 fuel rod response during a double-ended cold leg break LOCA [1].

Historically, LOCA safety analyses have been specifically tailored to prevent catastrophic fuel rod failure and ensure that the core remains controllable and amenable to long-term cooling. This approach relies on the ability of Zircaloy to maintain ductility following the reflood (i.e., quench) phase. The PQD of Zircaloy has been determined experimentally by exposing cladding ring samples to steam ($<1,204^{\circ}\text{C}$) for a period of time before quenching the sample at some temperature $<800^{\circ}\text{C}$. Cladding ductility is measured by performing a ring compression test and measuring the accumulation of permanent strain before failure at $\sim 135^{\circ}\text{C}$ and a predefined displacement rate of 0.033 mm/s [1]. These data suggest that PQD can be maintained, provided the oxide thickness or H concentration remains below an acceptable value and the peak cladding temperature (PCT) remains below $1,204^{\circ}\text{C}$. These requirements are outlined in 10 CFR 50.46, “Acceptance Criteria for Emergency Core Cooling Systems for Light-Water Nuclear Power Reactors.” Note that cladding burst behavior is not licensing criteria. These requirements have been sufficient to adequately protect public safety for existing operating practices; however, the US nuclear industry plans to extend the peak rod-average burnup beyond 62 GWd/tU . Extending burnup introduces new technical challenges where existing guidance may no longer be applicable. The most prominent technical challenge is associated with fuel fragmentation, relocation, and dispersal (FFRD), as well as its potential consequences.

FFRD was originally observed in high-burnup LOCA experiments performed at the Halden Boiling Water test reactor. These tests were originally designed to evaluate the effect of relocated fuel on local cladding temperatures; however, a LOCA test performed on fuel with a rodlet average burnup of $\sim 92\text{ GWd/tU}$ experienced extensive fragmentation to the point of pulverization, termed *high-burnup fuel fragmentation* (HBFF). Ultimately, the pulverized material relocated into the balloon region and dispersed through the cladding rupture opening. Since then, high-burnup LOCA test programs have investigated

this phenomenon and determined a burnup range (62–75 GWd/tU rod average) in which HBFF becomes relevant [9]. These experimental observations coupled with the US nuclear industry’s desire to extend burnup prompted the US Nuclear Regulatory Commission (NRC) to release a research information letter (RIL) to provide a basis to limit FFRD throughout the core based on interpretations of experimental findings.

The NRC RIL summarizes the Office of Nuclear Regulatory Research’s interpretation of FFRD experimental findings with the goal to define conservative thresholds for FFRD phenomena. The RIL highlights five elements with supporting technical bases for the industry to consider in its FFRD safety analysis. The elements are as follows: (1) fragmentation and pulverization threshold, (2) local cladding strain threshold, (3) mass susceptible to dispersal, (4) impact of transient fission gas release (FGR) on balloon burst behavior, and (5) basis to support packing fractions in the non-dispersed balloon region. The industry is pursuing multiple approaches to address FFRD from a safety analysis perspective. The simplest approach is to prevent burst from occurring; however, if burst does occur, then cladding performance (i.e., rupture timing, balloon size, and rupture size) will significantly affect FFRD and its consequences. Therefore, it may be critical to accurately model cladding ballooning during a LOCA. Modeling efforts to date have prioritized accurately predicting burst timing using the Chapman failure correlation. Comparisons between the calculated and experimentally measured balloon strains have been made, and the modeling results generally grossly underpredict post-burst peak cladding balloon strain (i.e., hoop strain). General consensus suggests that uncertainty in code predictions are related to varying experimental surface conditions, such as azimuthal or axial temperature gradients, that cannot be accurately captured because of a lack of experimental data.

Recent work at Oak Ridge National Laboratory (ORNL) used digital image correlation (DIC) and infrared (IR) thermography to assess Zircaloy cladding performance under a simulated loss-of-coolant transient condition. The developed capability generally provides high-fidelity time- and spatially dependent strain, strain rates, and temperature measurements. Therefore, this paper leverages in situ data generated from a simulated LOCA in the Severe Accident Test Station at ORNL to validate the BISON fuel performance code and the Zircaloy high-temperature creep model predictions. Additionally, this paper identifies and discusses model limitations. Lastly, this paper validates BISON for a simulated high-burnup LOCA test performed at ORNL.

2. VALIDATION TO IN SITU CLADDING BURST TESTS

2.1 DIGITAL IMAGE CORRELATION BURST TESTS SUMMARY

Eight DIC tests were performed at ORNL under the Advanced Fuels Campaign program, and five additional tests were identified from the literature [3–5]. The nominal pre-transient geometry for each test had a 9.5 mm outer diameter, 0.575 mm wall thickness, and 76 mm length. The test from the literature was ~210 mm long. For the ORNL test, cladding deformation was monitored through a ~38 mm hole bored through the side of the IR furnace. This enabled direct line of sight to the cladding tube through the viewing chamber. However, the cladding segment was shortened from the standard ~300 mm to 76 mm to ensure that the balloon evolution was visible. A thick-walled 316SS extension tubing was used to center the cladding directly in front of the viewing chamber. Each test was performed in air because the quartz reaction tube emitted IR as the temperature increased, rendering the cladding no longer visible. Finally, a SiC shell was used to smooth the axial and azimuthal temperature profiles by preventing the IR lamps from directly reflecting off the cladding surface. This addition enabled the cladding temperature along the axis to be accurately quantified because the IR reflections were no longer present. Table 1 and Table 2 summarize the ORNL and literature DIC tests. One important difference between the test described in Table 1 and the test described in Table 2 is that Table 2 used an internal W heater rather than an external IR furnace.

Table 1. Burst DIC test matrix.

Material	Specimen length (mm)	Heating rate (°C/s)	Heating type	Initial pressure at 20°C (MPa)	Pressure valve
Zry-4	76	1	External IR	6.2	Closed
				8.2	Closed
				10.3	Closed
				15.6	Closed
				6.2	Open
				8.2	Open
				10.3	Open
			15.6	Open	

Table 2 DIC tests from literature.

Material	Specimen length (mm)	Heating rate (°C/s)	Heating type	Initial pressure at 20°C (MPa)	Pressure valve	Reference
Zry-4	210	~1	Internal W heater	7	Open	3
		1		8	Open	4
		14		8	Open	4
		28		8	Open	4
		~1		7	Open	5

2.2 MODELING APPROACH

DIC LOCA tests outlined in Table 1 and Table 2 are intended to provide highly characterized data from a highly controlled test. The highly characterized data are intended to be used in a fuel performance code to provide time-dependent validation of the fuel performance code models. The BISON fuel performance code was used for the LOCA simulations described herein based on previous validation of the code for light-water reactor (LWR) applications [10–12]. BISON was built on the Multi-Physics Object-Oriented Simulation Environment (MOOSE) framework, which is a parallel finite element computational system [13]. MOOSE uses the Jacobian-free, Newton–Krylov (JFNK) method to solve fully coupled systems of nonlinear partial differential equations. Additionally, BISON can be parallelized to perform high-fidelity modeling of fuel rods in three dimensions, as well as in full-length *R-Z* and planar slice geometries. BISON has been extensively validated for both LWR steady-state [14] and transient [15] integral tests. The models used for these validation efforts are well documented [14, 15], as are the implementations of these models in BISON [6]. Table 3 summarizes the models used in BISON analysis and the associated references. The model leverages BISON’s *R-Z* capability with a 9.5 mm outer diameter and 0.575 mm wall thickness. The cladding length was different for the two different test conditions, and the BISON model accounts for these differences.

Table 3. Summary of the BISON models and associated references relevant to FFRD.

Fuel			Cladding		
Property	Model	Reference	Property	Model	Reference
Thermal conductivity	NFIR	[17, 18]	Thermal conductivity	Fink	[26]
Elastic properties	MATPRO	[19]	Elastic properties	MATPRO	[19]
FGR	Sifgrs	[20]	Thermal expansion	MATPRO	[27]
Thermal expansion	Constant	[21]	Thermal creep	Limback-Anderson and Erbacher	[19]
Pulverization	Turnbull	[33]	Rupture criteria	Chapman/strain rate	[28, 29]
			Rupture opening	NEAMS	[31]

The main consideration aside from tube geometry is associated with the simulated boundary conditions, and the DIC tests were developed with this in mind. Rod internal pressure was experimentally measured during the test by a pressure transducer. In a true validation framework, BISON would calculate the initial pressure at a specified temperature; however, the purpose of this comparison is to completely isolate the high-temperature creep model. Therefore, the experimentally measured pressure was directly applied to the inner surface of the tube. PCT was measured using a thermocouple located on the top of the cladding tube. An example of the measured pressure and PCT is shown in Figure 2. The axial temperature profile was determined by using an IR camera, and the thermocouple measurement provides a reference temperature for the IR camera. Two predominant axial temperature profiles were measured during the DIC tests, as shown in Figure 3. Figure 3 reports these temperature profiles in terms of a normalized value in accordance with the thermocouple measurement. The axial profiles shown in the figure are a direct result of sample location within the furnace, the hole in the furnace contributing to a local depression in the middle of the tube, and the SiC shell to normalize azimuthal temperatures. The appropriate axial temperature profile was applied to the exterior cladding surface for each DIC simulation. Finally, the DIC tests were unique insofar as the top and bottom of the tube were fixed, requiring the application of the appropriate BISON boundary conditions to prevent unrealistic axial displacements.

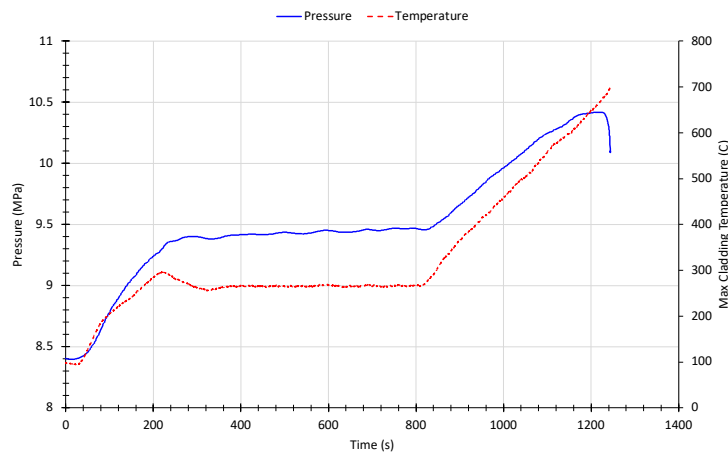


Figure 2. Time-dependent pressure and maximum temperature measurements during DIC LOCA test.

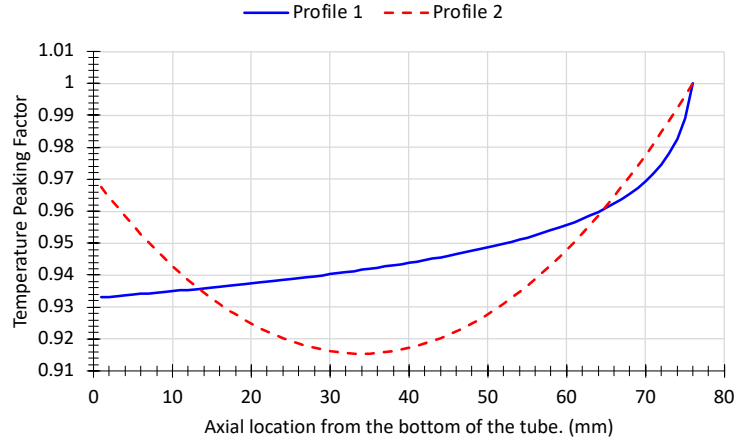


Figure 3. Cladding surface peaking factors measured by the IR camera at the time of burst.

2.2.1 High-Temperature Creep Model

The high-temperature cladding creep model implemented into BISON was first documented in Erbacher et al. [1] in 1980. The model was developed from isothermal uniaxial tension tests conducted in an inert atmosphere. The samples were directly heated with either a joule or ohmic system. A hydraulic system was used to apply a constant uniaxial load to the sample and measure strain under constant temperature and load conditions. Strain was determined by assessing the displacement of the hydraulic system as a function of time. The creep test was terminated after 10 min or a total strain of 0.15 (15%). Using these data in LOCA applications results in multiple concerns. First, Zircaloy is an anisotropic material due to its hexagonal close packed crystal structure. Nuclear-grade Zircaloy tubes are inherently anisotropic as a result from the crystal structure. Second, cladding burst tests inherently apply a biaxial stress state to the cladding tube material under dynamic temperature and pressure (i.e., stress) conditions. The data generated through the uniaxial tension test generate steady-state axial creep data under isothermal conditions; therefore, these data are applicable only under steady-state conditions in the axial direction. Furthermore, tube pressures in high-burnup fuel rods range from 8 to 15 MPa and possibly higher in some cases. Using thin wall approximation, the stress can range from ~70 to 125 MPa in the hoop direction and 25 to 60 MPa in the axial direction. However, the uniaxial creep data focus on low stresses (<60 MPa) at temperatures >700°C, and this trend is also true for biaxial creep data [7]. This strongly suggests that these data will not be applicable to simulated LOCA conditions with high rod internal pressure, like those expected in high-burnup fuel. Nonetheless, the uniaxial tensile data were used to generate the isotropic material parameters for uses in the following creep equation:

$$\dot{\epsilon}_{eff} = A \exp\left(\frac{-Q}{RT}\right) \sigma_{eff}^n, \quad (1)$$

where $\dot{\epsilon}$ is the effective creep strain rate, A is the strength coefficient ($\text{MPa}^{-n} \text{s}^{-1}$), Q is the activation energy (J/mol), T is the temperature (K), σ_{eff} is the effective stress (MPa), and n is a dimensionless stress exponent. The aforementioned data were used to estimate the material parameters for use in the creep equation shown in Table 4. More details of steady-state uniaxial creep testing are discussed in Rosinger et al. [8]. Information related to biaxial steady-state creep testing is discussed in Donaldson and Healey [7].

Table 4. Zircaloy-4 high-temperature creep material parameters [8].

Zircaloy phase	Creep rate regime	A ($\text{MPa}^{-n} \text{s}^{-1}$)	Q (J/mol)	n
α phase	—	8,737	$3.24e5 + 24.69(T - 923.15)$	5.89

Mixed $\alpha - \beta$ phase	$\dot{\epsilon}_{eff} \leq 3e-3$	0.24	1.02366e5	2.33
Mixed $\alpha - \beta$ phase	$\dot{\epsilon}_{eff} \geq 3e-3$	Interpolation	Interpolation	Interpolation
β phase	—	7.9	1.41919e5	3.78

2.3 BISON VALIDATION OF EXPERIMENTAL DATA

The aforementioned BISON fuel performance code and creep model were used to evaluate all DIC burst tests described in Table 1 and Table 2. However, this section discusses specific cases to highlight differences between simulations with low and high pressure and heating rates. A mechanistic creep model should consider the cladding stress state, temperature, or heating rate; therefore, evaluating bounding conditions should provide a reasonable summary of the model’s capabilities.

Figure 4 compares BISON modeling predictions with the experimentally measured DIC data for a 6.2 MPa open valve test. This case was selected for comparison because the pressure was held constant for the duration of the test, which ensures that the comparison is performed so that the creep model predictions are fully isolated at a specific rod internal pressure. The first observation is BISON generally overpredicts the experimentally measured values. The experimental values at temperatures lower than $\sim 600^\circ\text{C}$ likely have larger uncertainties due to the laser engravings (i.e., pattern fidelity) on the Zry-4, as well as potential heat waves causing changes in the optical path. In the future, a speckled pattern from high-temperature spray paint will be used to increase the fidelity of the DIC tracking field and reduce experimental uncertainties. However, BISON clearly overpredicts strain deformation above $\sim 600^\circ\text{C}$ to the point where the terminal strain values are $\sim 25\%$ greater than the experimentally measured value. Another interesting observation is related to the axial strain results. Generally, the measured axial strain values are near zero. This is related to the restraint applied to the top and bottom of the test train. The restraint is imperfect, and thus slight increases in the axial strain are observed. Perfect restraint of the test train would look similar to the BISON results with the axial strain being effectively zero until ballooning occurs. The axial strain becomes negative as large balloon deformation occurs. As the balloon radially expands, the tube is expected to axially contract—a behavior captured by BISON. Generally, some work may be required to improve the model as it relates to low-pressure conditions. However, the difference between the code predictions and experimentally measured values could fall within an appropriate deviation, and additional data may result in slight underpredictions.

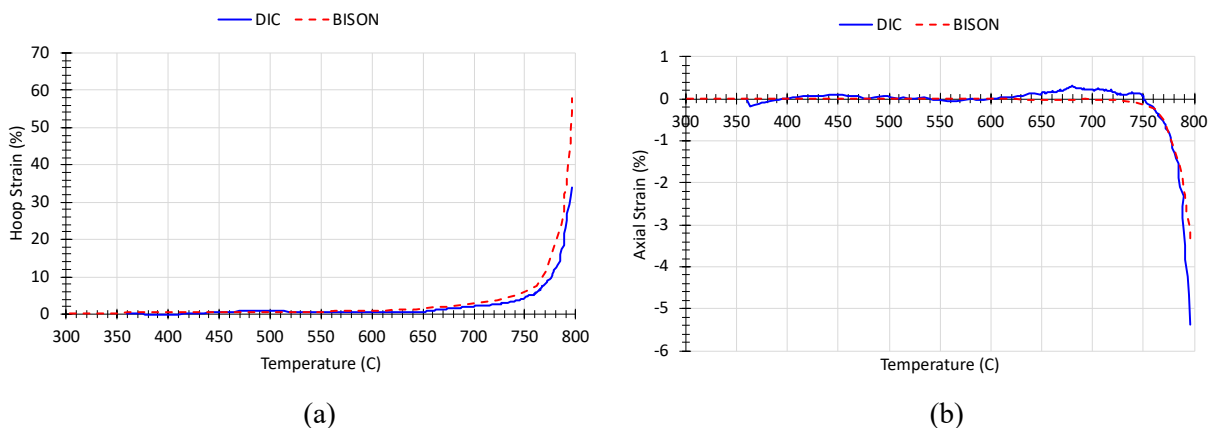


Figure 4. BISON (a) hoop strain and (b) axial strain comparison of DIC measurements from a constant low-pressure (6.2 MPa) DIC test.

Figure 5 presents similar results to those shown in Figure 4; however, the results in Figure 5 reflect a constant high pressure (15.1 MPa) Severe Accident Test Station (SATS) test. A pressure of 15.1 MPa is intended to represent a near-upper bound rod internal pressure that could be experienced by high-burnup (>62 GWd/tU rod average) fuel. Unlike the lower pressure comparison in Figure 4, BISON shows more deviation from the experimentally measured values, specifically hoop strain. This is unsurprising because the creep model was developed from a uniaxial creep test in which the applied stress is much lower than the internal pressure imposed on the cladding. Therefore, when extrapolating the empirical model to higher stresses, it is expected that the model would either over- or underpredict the experimental results. This deviation indicates that the current model is inappropriate for handling extreme pressure regimes, and model development is needed to more accurately capture high-pressure burst conditions. The deviation in the axial data in Figure 5(b) is a result of the high pressures and transient conditions that affect the test strain stability. Again, a perfect constraint would result in a near-zero axial strain until ballooning occurs.

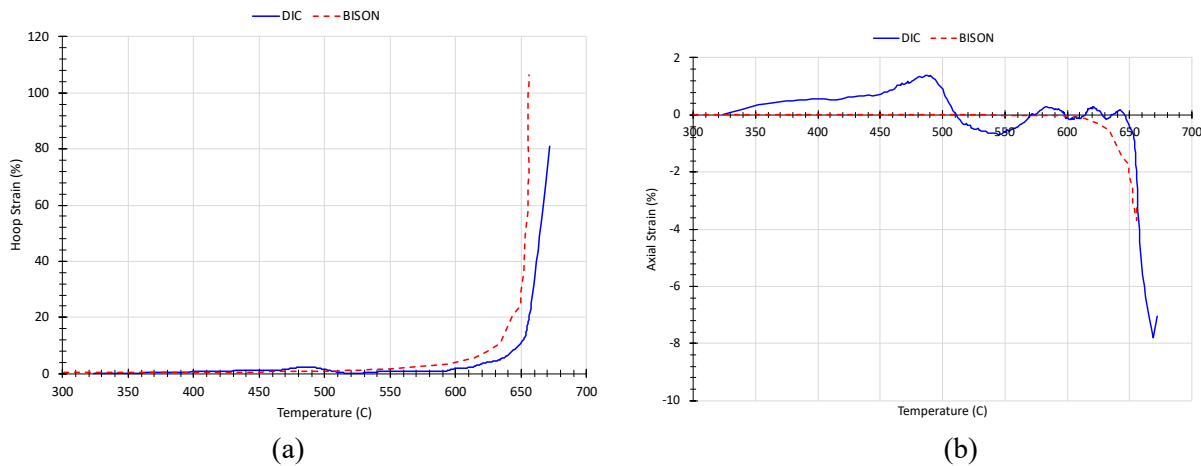


Figure 5. BISON (a) hoop strain and (b) axial strain comparison of DIC measurements from a constant high-pressure (15.1 MPa) DIC test.

A second comparison is shown in Figure 6. In the figure, the pressure is held constant at 8 MPa, and the heating rate is varied. The heating rate in Figure 6(a) is 1°C/s, whereas the heating rate in Figure 6(b) is 28°C/s. The results in Figure 6(a) show good agreement between BISON predictions and the experimental data; however, the results disagree as temperature increases, likely because of tertiary creep. Again, this is unsurprising because the data used to develop the creep model are from a slow experiment that lasted ~15 min with similar stress conditions. However, the model performs poorly in the higher heating rate conditions, as shown in Figure 6(b). The model initially overpredicts strain, and this behavior continues until the experimental data suggest the presence of plastic instability, resulting in rapid changes in the strain behavior. BISON predictions suggest a slower strain response than the experimental data, and the trend of overpredicting reverses as temperature increases. This indicates a heating rate model deficiency and affects the ability of the empirical model to accurately predict balloon deformation under high heating rate conditions.

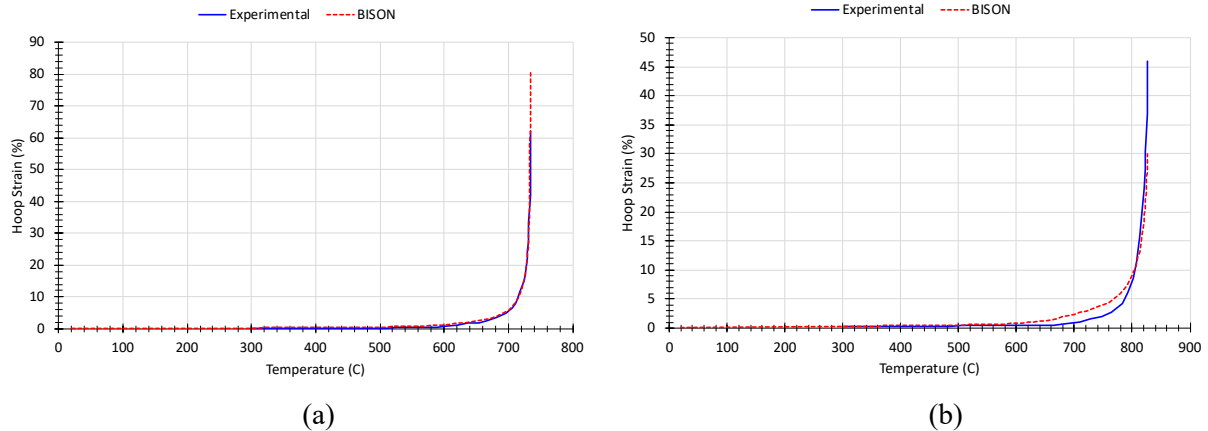


Figure 6. BISON hoop strain comparison as a function of heating rates to DIC measurements from a constant pressure (8 MPa) DIC tests at (a) 1°C/s and (b) 28°C/s.

The results compare two similar cases; however, in reality, cladding balloon and burst behavior are statistical in nature. Therefore, BISON was used to assess every case reported in Table 1 and Table 2 to determine the difference between the BISON results and the experimental data from a broader statistical evaluation. BISON results and experimental data were extracted at the same at temperatures for direct comparison. The percent difference was determined by subtracting the experimental data from the BISON predictions and dividing by the measured data. This comparison illuminates differences between the model predictions and identifies modeling gaps or areas of high uncertainties within the model. Figure 7 illustrates this comparison as a function of temperature. Additionally, the data are divided into various components; blue circles represent heating rates greater than 1°C/s, red triangles represent pressures greater than 9 MPa, and green squares represent data for which the heating rate equals 1°C/s and the internal pressure is less than 9 MPa. There is generally significant scatter in the data, and most of the data suggest that BISON overpredicts the experimentally measured data. Again, the experimental data at temperatures <500°C may be subject to measurement uncertainties given that the measured strain values are close to 0.1%. However, trends in the data are clear. BISON overpredicts (>100%) high heating rates (>1°C/s) at lower temperatures; however, the trend reverses as the temperature increases, as shown in Figure 6(b). The most notable trend is observed for high rod internal pressures (>9 MPa). BISON is reasonably successful at predicting strains at lower temperature. However, as the temperature exceeds ~500°C, BISON overpredicts the experimental results by 200%. This is unsurprising because BISON generally overpredicts strain; moreover, the model's range of applicability does not extend to high pressures (>9 MPa). The model extrapolates from its range of applicability to the high-pressure conditions, and as the results indicate, the extrapolation further deviates from the experimental data. However, the model is reasonably successful at predicting strain evolution where the heating rate equals 1°C/s and the pressure is less than 9 MPa. The culmination of these results suggests that the high-temperature creep model currently used in BISON needs improvement. The first-order improvements ensure that the model better handles higher heating rates (>1°C/s) and higher pressures (>9MPa). The second-order improvements ensure that the model considers microstructure evolution before and during the LOCA transient.

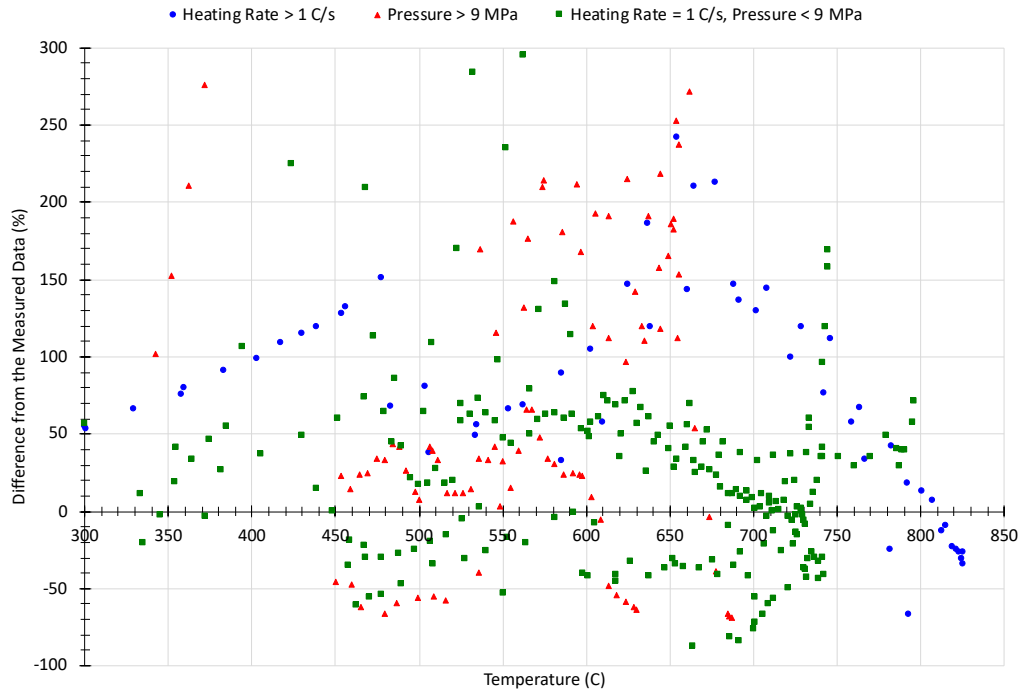


Figure 7. Percent difference between the BISON predictions and experimentally measured (P-M)/M.

Lastly, BISON stress rate– and strain rate–based failure and hoop strain predictions were compared with the experimentally measured values in Table 5. The stress-based failure model is model reported in NUREG 0630 [1], whereas the strain-rate failure model occurs when the strain rate is greater than 2.78 %/s [34]. The stress-based failure model generally predicts a lower failure temperature than the strain rate failure model for a heating rate of 1°C/s and also underpredicts hoop strain. The strain rate model predicts failure with reasonable success, and hoop strain results are poor, except for two cases. In several cases, the strain rate failure model does not predict failure. However, this does not indicate limitations of the failure model but instead highlights the limitations within the creep model. These results indicate that the strain rate failure models provides better predictions with respect to the experimental data. However, the behavior reverses as heating rate increases. This is expected because the stress-based failure criterion is a function of the heating rate, whereas the strain-rate failure criterion does not have a heating rate dependence, which suggests that additional data are needed to refine the applicability of the strain rate failure model.

Table 5. BISON rupture predictions in comparison to the experimentally measure values

Initial pressure at 20°C (MPa)	Pressure valve	Heating rate	Experimental rupture temperature (°C)	Experimental rupture strain (%)	Rupture temperature (°C): stress-based failure	Rupture strain (%): stress-based failure	Rupture temperature (°C): strain-rate based failure	Rupture strain (%): strain rate-based failure
6.2	Open	1	796	34	771	11	791	34.8
7	Open	1	687*	68	N/A	12	N/A	12
7	Open	1	642*	100	N/A	12	N/A	12
8	Open	1	735	62	703	6	711	8.3
8.2	Open	1	751	84	720	10.3	741	46.6
10.3	Open	1	687	49	674	7.8	N/A	15.1
15.9	Open	1	671	66	566	2.2	652	47.5
6.2	Closed	1	739	34.5	N/A	12	N/A	12
8.2	Closed	1	703	58	662	6	N/A	16.4
10.3	Closed	1	681	62	674	7.8	N/A	15.1
15.9	Closed	1	631	30	545	1	N/A	10.9
8	Open	14	793	40	776	16	768	5
8	Open	28	826	46	802	23	781	6

*Sample was not heated to rupture due to internal W heater

3. BISON VALIDATION TO HIGH-BURNUP LOCA TEST

3.1 HIGH-BURNUP LOCA TESTING AT ORNL

The SATS—which is installed at the Irradiated Fuels Examination Facility, a hot cell facility at ORNL—is an integral test facility capable of studying the response of irradiated fuels and materials under design basis accident (DBA) and beyond DBA (BDBA) scenarios. The motivation behind the development of this capability is restoring the US capability to perform semi-integral LOCA testing on irradiated materials. An overview of the test station before in-cell insertion is provided in Capps et al. [9], and Table 6 summarizes the range of test parameters for each type of SATS test.

Table 6. Summary of test parameters for each module and test type.

	DBA module		BDBA module
	LOCA integral test	Oxidation-quench test	High-temperature test station
Sample spec	Fueled rod	Defueled rod	Rod or coupon with 3 mm hole
Sample segment (mm)	~200–300	~25–50	~25–50
Pressure (MPa)	~8, maximum 20	0.1	0.1
Max temp (°C)	1,200	1,200	1,700
Heating rate (°C/s)	5	5, maximum 20	0.25, maximum 0.33
Steam flow rate (mg/cm ² ·s)	~5.7	~5.7	3.0–7.0
Gas environment	Steam or Ar	Steam or Ar	Steam or Ar
Quench (°C)	At 20–800	At 20–800	None
Quench condition	Rising water around sample	Rising water around sample	None
Quench flow rate, mm/s	≥15	≥15	None
Test time, min	≥30	≥30	Multiple days

This strategic capability emerges as the US nuclear power industry is under financial duress due to low natural gas prices; as a result, several plants have shut down. The nuclear industry has since progressed toward extending burnup beyond 62 GWd/tU in an effort to reduce operational cost and alleviate financial duress. However, the NRC has identified FFRD as a crucial issue that must be addressed for burnup extension. To date, three high-burnup LOCA tests have been performed in SATS [9].

The high-burnup test specimens were assembled with two Type-S thermocouples strapped to the outer surface of the cladding at ~5 cm above the sample centerline. The LOCA tests were conducted in a steam environment at 1,000°C but without water quench. The full LOCA sequence is as follows:

- Heat in flowing steam to 300°C and pressurize fuel segment to 1,200 psi
- Heat in flowing steam at 5°C/s from 300°C to 1,000°C
- Hold in steam for 120 s at 1,000°C
- Cool at 3°C/s to 800°C
- Furnace cool from 800°C to room temperature

Figure 8 highlights the experimentally measured temperature and pressure from the North Anna (NA) 1 high-burnup LOCA test.

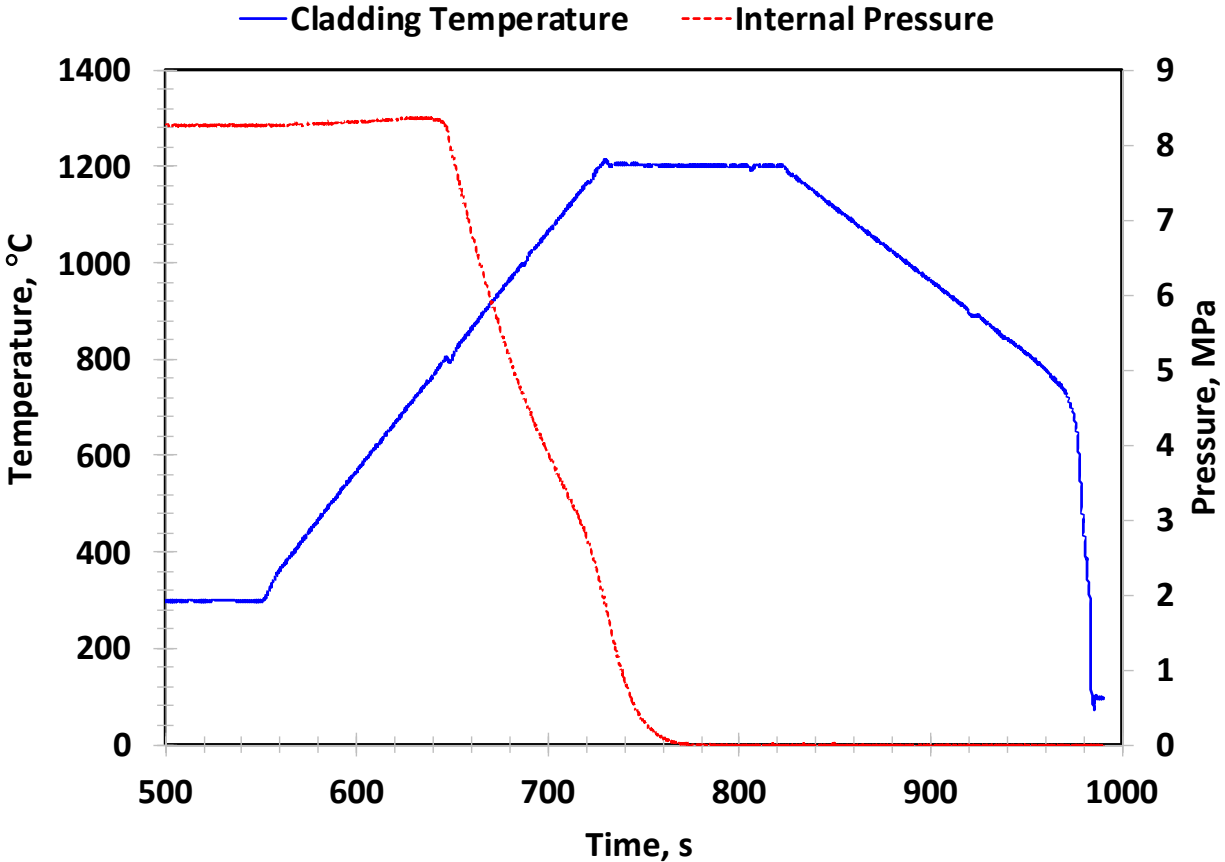


Figure 8. Cladding temperature and tube pressure recorded during the NA 1 high-burnup LOCA test [9].

3.2 BISON VALIDATION OF EXPERIMENTAL DATA

3.2.1 HB Robinson

A high-burnup fuel rod segment was harvested from a fuel rod irradiated in the HB Robison PWR for postirradiation examination and subsequent LOCA testing. The characteristic fuel rod geometry is shown in Table 7. The fuel rod design is specific to a 15×15 fuel assembly design, and this fuel rod is of an older design. More modern PWR fuel designs comprise thinner cladding tubes, smaller outer diameters, and modern cladding alloys. The fuel rod properties shown in Table 7 were used to develop a representative BISON model to provide accurate fuel performance and depletion results before simulating the LOCA test results. The rodlet was harvested from the axial location spanning 2.54–2.84 m from the bottom of the fuel rod. This segment was specifically chosen because of the relatively flat burnup profile and because the local power is slightly higher than the rod average linear heat rate. The fuel rod power history was extracted from Gerzack et al. [32] and reproduced in Figure 9. The fuel rod was operated irradiated for five cycles in a relatively low-power location. After the five cycles, the rod was pulled out and inserted into a new assembly for a sixth and seventh cycle until its final discharge in 1995.

Table 7. HB Robinson segment characteristics used to develop BISON steady-state and transient models.

Reactor type	PWR
Initial enrichment (wt % ²³⁵ U)	2.9
Segment average burnup (GWd/tU)	71
Discharge year	1995
Cladding type	Zircaloy-4
Cladding outer diameter (mm)	10.76
Wall thickness (mm)	0.76
Pellet outer diameter (mm)	9.06
Pellet-cladding gap thickness (mm)	0.095

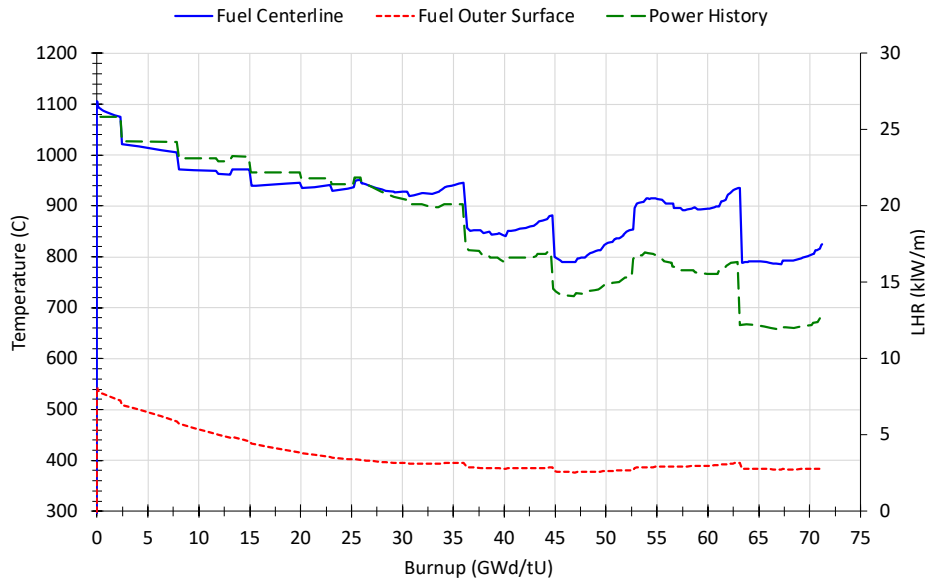


Figure 9. BISON power history and fuel temperature results as a function of rodlet average burnup [32].

Based on the rodlet operational history, the fuel temperatures and FGR would be expected to be low. BISON fuel centerline and periphery temperature predictions confirm this hypothesis, as shown in Figure 9. The fuel centerline temperature follows the linear heat rate as expected, whereas the pellet periphery temperatures decrease to a near-equilibrium temperature that is ~75°C higher than the reactor coolant temperature. The pellet periphery temperature evolution is constant, and gap closure occurs early in life. BISON predicts minimal FGR, whereas the experimentally measured fission gas on a full-length fuel rod was 2.1% [32]. Subsequently, BISON was used to simulate the SATS LOCA test of this rodlet to assess fuel fragmentation predictions. Details about the HB Robinson test conditions are provided in Capps et al. [9].

Two different rupture models were considered for the BISON evaluation. The first leverages a stress-based failure criteria developed and used by the NRC [28], whereas the second model uses the cladding strain rate to determine failure [29]. The two models should result in different cladding deformation at rupture and provide a lower and upper bound on predicted cladding deformation. Cladding rupture during the experiment occurred at 770°C, and both failure models overpredicted the rupture temperature: 780°C and 787°C with the stress-based failure criteria being lower. However, the predicted peak cladding

deformation behavior for both rupture conditions differs significantly from the experimentally measured value, as shown in Figure 10. BISON predictions suggest that the peak cladding hoop strain will remain below 10%, whereas the experimental data double the BISON predictions. This suggests that BISON is not accurately accounting tertiary creep and tertiary creep's effect on cladding deformation. However, this is be useful only if the strain-rate failure criteria were being considered because the stress-based approach fails before tertiary creep could occur. Transient FGR (tFGR) was not considered in the LOCA simulation. However, the measured rod internal pressure was directly applied to the tube's inner surface. Therefore, any tFGR would have been captured in the simulation.

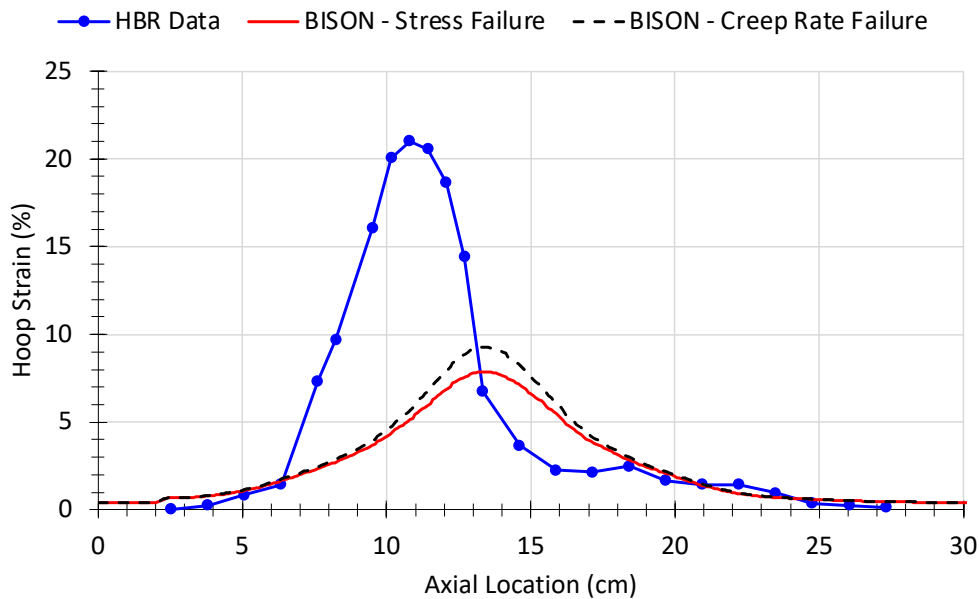


Figure 10. BISON post-LOCA cladding hoop strain results for the stress-based and strain cladding failure criteria [9].

The NRC's RIL outlines thresholds for calculating FFRD. The primary thresholds of interest are for fuel fragmentation and cladding strain threshold below which fuel relocation is limited. The fuel fragmentation criteria outlined in the NRC RIL are twofold. The first, shown in Eq. (2), is for fragments smaller than 1 mm. The second, shown in Eq. (3), is for fragments smaller than 2 mm. The only input parameter is the local or rodlet average burnup, shown as Bu.

$$\text{Mass Fraction} = 0.04(\text{Bu}-55), \quad (2)$$

$$\text{Mass Fraction} = 0.05(\text{Bu}-55), \quad (3)$$

Additionally, a second empirical model was developed by Turnbull [33] and is based on the local/nodal burnup of the sample, as well as terminal temperature. Turnbull's model is applicable only to fragments smaller than 1mm, and for the purposes of this analysis, only fragments smaller than 1 mm are discussed. The second threshold is the cladding relocation threshold based on cladding strain. The RIL suggests that fuel relocation will be mitigated if the cladding strain remains below 3%. Table 8 shows the results of the analysis when comparing the Turnbull and RIL fragmentation criteria, as well as an estimate of how much fuel will be susceptible to relocation and potential dispersal. The RIL clearly overestimates the amount of fragmented material, whereas the Turnbull model is within 3% of the experimentally measured data. When applying the 3% strain restriction on relocation, both results drop by one-third. The

experimental data have a large peak value, but the hoop strain along the axis is 9 cm, whereas the BISON results are 10 cm. Therefore, this value is considered more conservative than the experimentally measured value, and this is also true when comparing the experimentally measured values to the values predicted.

Table 8. Summary of the BISON models and associated references relevant to FFRD.

	Turnbull fragmentation criteria	RIL fragmentation criteria (1 mm/2 mm)
Fuel susceptible to pulverization (%)	30.6	64/80
Fuel susceptible to relocation (%)	10.2	21/27
Measured fragmentation = 31.56%		
Calculated fuel susceptible to relocation = 9.4%		

3.2.2 North Anna

A high-burnup fuel rod segment was harvested from a fuel rod irradiated in the NA PWR for postirradiation examination and subsequent LOCA testing. The characteristic fuel rod geometry is shown in Table 9. The fuel rod is from a more modern fuel rod and assembly design, but very little is known about the operating conditions. The last cycle power was estimated to be above 15 kW/m, and the rodlet in question was harvested 1.83–2.28 m from the bottom of the fuel rod. It would be reasonable to suggest that this rodlet was operating between 19 and 21 kW/m at end of life; however, this is merely speculation. Therefore, BISON was used to evaluate only the LOCA transient portion of the evaluation.

Table 9. NA segment characteristics used to develop BISON transient models

Reactor type	PWR
Initial enrichment (wt % ²³⁵ U)	4.2
Segment average burnup (GWd/tU)	69
Discharge year	2004
Cladding type	M5
Cladding outer diameter (mm)	9.5
Wall thickness (mm)	0.57
Pellet outer diameter (mm)	8.2
Pellet-cladding gap thickness (mm)	0.080

BISON NA predictions are similar to the HB Robinson results in that BISON significantly underpredicted the peak hoop strain. Again, two failure criteria were considered in the analysis, and both underpredicted hoop strain. However, the one significant difference between the NA and HB Robinson results is that the NA sample ruptured at 791°C, and BISON predicted rupture to occur at 753°C (stress-based criteria) or 760°C (strain rate). The decrease in the burst prediction is related to the change in cladding thickness: HB Robinson had a cladding thickness of 0.74 μm, and NA has a cladding thickness of 0.57 μm. Other factors, such as oxide thickness, may have contributed to the difference in rupture. Because HB Robinson was Zirclaoy-4, it had a large oxide (~100 μm), whereas the NA rodlet had an oxide layer of ~30 μm. Nonetheless, BISON still significantly underpredicted the balloon geometry, and unlike the HB Robinson results, the axial balloon geometry is less than the experimentally measured values. This is most likely due to differences in axial temperature gradients along the tube along with a lack of tertiary creep being appropriately captured.

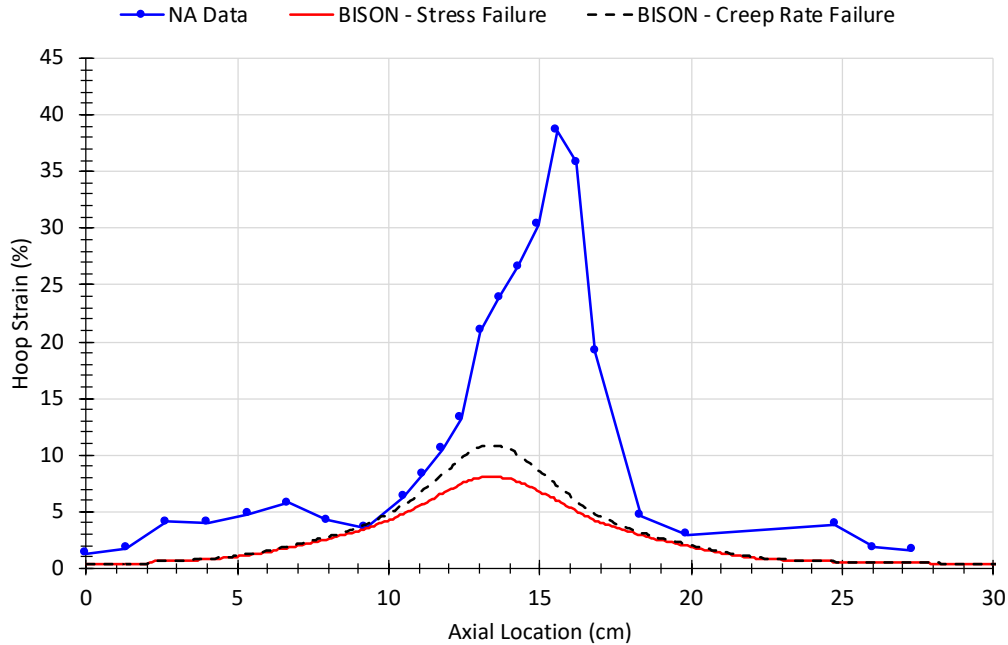


Figure 11. BISON post-LOCA cladding hoop strain results for the stress-based and strain cladding failure criteria.

A similar fuel fragmentation calculation was performed on the NA sample. The Turnbull model predicts similar mass fraction of fragmentation <1 mm that is within 13% of the experimental values, whereas the RIL model grossly overpredicts the amount of fragmented fuel. However, the calculated balloon geometry significantly affects the result: the experiment balloon length was twice that calculated by BISON. Again, this may be a thermal boundary issue, and it may also be a function of BISON’s inability to consider tertiary creep and predict the peak hoop strain.

Table 10. Summary of the BISON models and associated references relevant to FFRD.

	Turnbull fragmentation criteria	RIL fragmentation criteria (1 mm/2 mm)
Fuel susceptible to pulverization (%)	23.4	56/70
Fuel susceptible to relocation (%)	7.8	18.7/23.3
Measured fragmentation = 27.4%		
Calculated fuel susceptible to relocation = 16.4%		

4. SUMMARY AND FUTURE WORK

BISON simulations were used to evaluate in situ DIC burst tests to assess the high-temperature creep model. The results suggest that the creep model is reasonably successful under very specific conditions, but when those conditions deviate, the model results also deviate. Conditions for which the model showed reasonable predictions occurred when the rod internal pressure remained below 9 MPa and the heating rate was equal to 1°C/s. The model did not perform well when high rod internal pressure or heating rates were considered. Subsequently, BISON was used to simulate LOCA testing on high burnup. Cladding deformation was evaluated, and fuel fragmentation was estimated based on guidance provided by the

NRC RIL on FFRD. The NRC guidance demonstrated a constant overprediction, whereas the Turnbull pulverization model predictions were comparable to the experimentally measure data.

The existing high-temperature creep model was determined to be generally unable to accurately predict balloon deformation during a simulated LOCA test. Cladding deformation has a statistical dependence, but through numerous comparisons, the model consistently highlighted significant gaps within the model. The first is the model's inability to accurately capture cladding behavior above 9 MPa. Because the model was not intended for use at such high pressure, model improvements are required to broaden the application of this model to higher pressures. Second, the model was unable to capture cladding deformation under high heating rate conditions. Similar to the pressure gap, the model was developed using uniaxial tensile tests under a constant load and temperature conditions. However, burst tests are transitory by nature, and the model appears inadequate in capturing the transitory behavior. Lastly, additional data under constant pressure conditions over a broad range of pressures would be invaluable to improving and validating the high-temperature creep model.

5. ACKNOWLEDGMENTS

This work was supported by the US Department of Energy's Nuclear Energy Advanced Modeling and Simulation (NEAMS) program. The authors express their appreciation to Caleb Massey for providing detailed technical feedback. His feedback helped improve the technical content of the report.

6. REFERENCES

1. F. Erbacher and S. Leistikow. 1987. "Zircaloy Fuel Cladding Behavior in a Loss-of-Coolant Accident: A Review." *Zirconium in the Nuclear Industry*, ed. R. Adamson and L. S. Van (West Conshohocken, PA: ASTM International 451–488.
2. M. Billone, Y. Yan, T. Burtseva, and R. Daum. 2008. *Cladding Embrittlement During Postulated Loss-of-Coolant Accidents*. NUREG/CR-6967. US NRC, Office of Nuclear Regulatory Research.
3. J. Kim, J. W. Yoon, H. Kim, and S.-U. Lee. 2021. "Prediction of Ballooning and Burst for Nuclear Fuel Cladding with Anisotropic Creep Modeling during Loss of Coolant Accident (LOCA)." *Nuclear Engineering and Technology* 53, no. 10. <https://doi.org/10.1016/j.net.2021.04.020>.
4. G.-H. Choi, D.-H. Kim, C.-H. Shin, J. Y. Kim, and B. Jae Kim. 2020. "In-Situ Deformation Measurement of Zircaloy-4 Cladding Tube under Various Transient Heating Conditions Using Optical Image Analysis." *Nuclear Engineering and Design* 370: 110859. <https://doi.org/10.1016/j.nucengdes.2020.110859>.
5. D.-H. Kim, G.-H. Choi, H. Kim, C. Lee, S.-U. Lee, J.-D. Hong, and H.-S. Kim 2020. "Measurement of Zircaloy-4 Cladding Tube Deformation Using a Three-Dimensional Digital Image Correlation System with Internal Transient Heating and Pressurization." *Nuclear Engineering and Design* 363: 110662. <https://doi.org/10.1016/j.nucengdes.2020.110662>.
6. J. D. Hales, R. L. Williamson, S. R. Novascone, G. Pastore, B. W. Spencer, D. S. Stafford, K. A. Gamble, D. M. Perez, and W. Liu. 2016. *BISON Theory Manual: The Equations behind Nuclear Fuel Analysis*. United States. doi:10.2172/1374503.
7. A. T. Donaldson and T. Healey. 1984. *Creep Deformation of Westinghouse Zircaloy-4 Fuel Cladding Tubes in Alpha Plus Beta Phase Temperature Range*. TRPD/B/056/N85, Central Electricity Generating Board, Berkely, Gloucestershire, United Kingdom.
8. H. E. Rosinger, P. C. Bera, and W. R. Clendening. 1979. "Steady-State Creep of Zircaloy-4 Fuel Cladding from 940 to 1873 K." *J. Nucl. Mater.* 82: 286–279.
9. N. Capps, Y. Yan, A. Raftery, Z. Burns, T. Smith, K. Terrani, K. Yueh, M. Bales, and K. Linton. 2020. "Integral LOCA Fragmentation Test on High-Burnup Fuel." *Nucl. Eng. Des.* 367: 110811.

10. R. L. Williamson, N. A. Capps, W. Liu, Y. R. Rashid, and B. D. Wirth. 2016. "Multi-Dimensional Simulations of LWR Fuel Behavior in the BISON Fuel Performance Code." *JOM* 68, no. 11.
11. R. Williamson, J. Hales, S. Novascone, M. Tonks, D. Gaston, C. Permann, D. Andrs, and R. Martineau. 2012. "Multidimensional Multiphysics Simulation of Nuclear Fuel Behavior." *J. Nucl. Mater.* 423: 149–163.
12. R. L. Williamson, K. A. Gamble, D. M. Perez, S. R. Novascone, G. Pastore, R. J. Gardner, J. D. Hales, W. Liu, and A. Mai. 2016. "Validating the BISON Fuel Performance Code to Integral LWR Experiments." *Nucl. Eng. Des.* 301: 232–244.
13. C. J. Permann, D. R. Gaston, D. Andrs, R. W. Carlsen, F. Kong, A. D. Lindsay... and R. C. Martineau. 2020. "MOOSE: Enabling Massively Parallel Multiphysics Simulation." *SoftwareX* 11: 100430.
14. R. L. Williamson, K. A. Gamble, D. M. Perez, S. R. Novascone, G. Pastore, R. J. Gardner, J. D. Hales, W. Liu, and A. Mai. 2016. "Validating the BISON Fuel Performance Code to Integral LWR Experiments." *Nuclear Engineering and Design* 301: 232–244.
<https://doi.org/10.1016/j.nucengdes.2016.02.020>.
15. R. L. Williamson, G. Pastore, B. W. Spencer, J. D. Hales, and T. Tverberg. 2017. "BISON Validation for LOCA and PCMI Behavior Using Measurements from the Halden Reactor Project," United States. <https://www.osti.gov/servlets/purl/1414448>.
16. J. D. Hales, R. L. Williamson, S. R. Novascone, G. Pastore, B. W. Spencer, D. S. Stafford, K. A. Gamble, D. M. Perez, and W. Liu. 2016. "BISON Theory Manual: The Equations behind Nuclear Fuel Analysis." United States. doi:10.2172/1374503.
17. S. Yagnik. 2000. "Thermal Conductivity Recovery Phenomenon in Irradiated UO_2 and $(U,Gd)O_2$." *Proc. of Int. Top. Mtg. on LWR Fuel Performance*, Parkcity, Utah.
18. M. Lippens and L. Mertens. 1996. *High Burnup UO_2 and $(U,Gd)O_2$ Thermal Diffusivity Measurements and Post-Irradiation Characterizations*. EPRI Report TR-106501.
19. L. J. Siefken, E. W. Coryell, E. A. Harvego, and J. K. Hohorst. 2001. *SCDAP/RELAP5/MOD3.3 Code Manual: MATPRO—ALibrary of Materials Properties for Light-Water-Reactor Accident Analysis*. NUREG/CR-6150, Vol. 4, Rev. 2. US Nuclear Regulatory Commission..
20. L. P. Swiler, R. L. Williamson, and D. M. Perez. 2013. "Calibration of a fuel relocation model in BISON." In *International Conference on Mathematics and Computational Methods Applied to Nuclear Science & Engineering*, Sun Valley, Idaho, May 5–9, 2013. American Nuclear Society.
21. G. Pastore, L. Luzzi, V. Di Marcello, and P. Van Uffelen. 2013. "Physics-Based Modelling of Fission Gas Swelling and Release in UO_2 Applied to Integral Fuel Rod Analysis." *Nuclear Engineering and Design* 256: 75–86.
22. K. Sakai. 2013. *The Fuel Creep Test IFA-701: Results after Four Irradiation Cycles*. HWR-1039. OECD Halden Reactor Project.
23. K. Sakai, H. Hanakawa, and T. Tverberg. 2011. *Investigation of Fission Induced Creep of UO_2 and Cr-Doped fuel in IFA-701*. HWR-1006. OECD Halden Reactor Project.
24. R. Szoke and T. Tverberg. 2014. *Update on In-Pile Results from the Fuel Creep Test IFA-701*. HWR-1092. OECD Halden Reactor Project.
25. G. Pastore, L. Luzzi, V. Di Marcello, and P. Van Uffelen. 2013. "Physics-Based Modelling of Fission Gas Swelling and Release in UO_2 Applied to Integral Fuel Rod Analysis." *Nuclear Engineering and Design* 256: 75–86.
26. J. K. Fink and L. Leibowitz. 1995. "Thermal Conductivity of Zirconium." *Journal of Nuclear Materials* 226: 44–50.

27. D. G. Franklin. 1982. "Zircaloy-4 Cladding Deformation during Power Reactor Irradiation." In *Zirconium in the Nuclear Industry*, ASTM International.
28. M. Limbäck and T. Andersson. 1996. "A Model for Analysis of the Effect of Final Annealing on the In- and Out-of-Reactor Creep Behavior of Zircaloy Cladding." In *Zirconium in the Nuclear Industry: Eleventh International Symposium*, ed. E. Bradley and G. Sabol, 448–468. West Conshohocken, Pennsylvania. ASTM International.
29. F. J. Erbacher, H. J. Neitzel, H. Rosinger, H. Schmidt, and K. Wiehr. 1982. "Burst Criterion of Zircaloy Fuel Claddings in a Loss-of-Coolant Accident." In *Zirconium in the Nuclear Industry, Fifth Conference*. ASTM STP 754, ed. D. G. Franklin ed., 271–283. American Society for Testing and Materials.
30. N. E. Hoppe. 1991. "Engineering Model for Zircaloy Creep and Growth." In *Proceedings of the ANS-ENS International Topical Meeting on LWR Fuel Performance*, 157–172. Avignon, France, April 21–24, 1991.
31. N. Capps and R. Sweet. 2022. "Model for Determining Rupture Area in Zircaloy Cladding under LOCA Conditions." *Nuclear Engineering & Design*, under review (2022).
32. T. J. Gerzack, C. M. Parish, P. D. Edmondson, C. A. Baldwin, K. A. Terrani. 2018. "Restructuring in High Burnup UO_2 Studied Using Modern Electron Microscopy." *Journal of Nuclear Materials* 509: 245–259. <https://doi.org/10.1016/j.jnucmat.2018.05.077>.
33. J. A. Turnbull et al. 2015. "An Assessment of the Fuel Pulverization during LOCA-Type Temperature Transients." *Nucl. Sci. and Eng.* 179: 1–5.
34. V. Di Marcello, A. Schubert, J. van de Laar, and P. Van Uffelen. 2014. "The TRANSURANUS Mechanical Model for Large Strain Analysis." *Nuclear Engineering and Design* 276: 19–29.